J Appl Electrochem (2013) 43:1017–1026
DOI 10.1007/s10800-013-0585-7

ORIGINAL PAPER

Differential capacity plot as a tool for determination of electroactive surface area within a PEMFC stack

Yohann Chatillon · Caroline Bonnet · François Lapicque

Received: 15 May 2013 / Accepted: 27 June 2013 / Published online: 10 July 2013

Abstract Voltammetric techniques are usually employed for characterization of PEM single cells in terms of fuel crossover and electrochemical active surface. These techniques are, however, no more valid for individual characterization of the cells forming a PEM stack. Previous works suggested the use of chronopotentiometric measurements with current pulses: various interpretations of the curves can be used for characterization of individual cells, with, however, different accuracy levels in the determination of the two above cell features. The present manuscript establishes the comparison of voltammetric and potentiometric techniques for characterization of three single cells of the same grade, then potentiometric measurements were carried out with the stack formed by the above cells. Interpretation conducted by differential capacity plots was shown to lead to accurate characterization of electrochemical features of the three cells as indicated by the agreement between voltammetric and potentiometric techniques for individual cells and the data obtained in the stack.

Keywords PEM fuel cells · Stack operation · Electrochemical active surface · Chronopotentiometry · Differential capacity

1 Introduction

Proton exchange membrane fuel cells (PEMFC) are energy conversion systems that appear promising as an alternative energy production tool. Because of their high efficiency, their convenient operation, and reduced emissions to the environment, these systems are considered as reliable tools for energy production in both stationary and mobile applications [1, 2]. However, durability, cost, and reliability of membrane electrode assemblies (MEA) do not allow—at the present time—large-scale commercialization of this system. More efforts must be done to better understand aging mechanisms in order to mitigate degradation within MEAs. Thus, stack level investigations focusing on the characterization of the individual cell composing the system are necessary to understand and improve its long-term performance.

Characterization of PEM single cells can be carried out by voltammetric techniques upon feeding of the cell with nitrogen and hydrogen to the anode and cathode sides, respectively. Linear sweep voltammetry (LSV) performed at low sweep rate gives access to hydrogen crossover [3] while cyclic voltammetry (CV) leads to the electrochemical active surface of the electrode [4]. Unfortunately, these potential control techniques are mostly limited to single cell configuration as explained below.

In stack configuration, the cells are electrically connected in series: according to Kirchhoff's law the current crossing each cell is the same. However, since the cells forming the stack are not strictly identical in terms of electrochemical properties their voltage responses to an electrical solicitation often differ from each another. In such systems, potential control techniques such as LSV or CV usually lead to an uneven distribution of the potential along the stack: some cells may not reach the desired or expected electrochemical solicitation which prevents their characterization. If a potential ramp is applied to a stack, the sweep rate measured at the terminals of the stack (v_{stack}) and the sweep rate imposed by the potentiostat

Y. Chatillon · C. Bonnet · F. Lapicque (✉)
Laboratoire Réactions et Génie des Procédés,
CNRS-Nancy University, 1 rue Grandville,
PO Box 20451, 54001 Nancy, France
e-mail: francois.lapicque@ensic.inpl-nancy.fr

($v_{control}$) are to be very close to each another—within experimental uncertainty:

$$v_{control} \cong v_{stack} \quad (1)$$

The sweep rate of the stack is the sum of the sweep rates of each cell:

$$v_{stack} = \sum_{cells} v_{cell} \quad (2)$$

However, the distribution of sweep rate in the various cells will not necessarily be uniform along the stack. Thus, if n is the number of cells composing the stack, the following relation holds:

$$v_{cell} \neq \frac{v_{stack}}{n} \quad (3)$$

For that reason, galvanic control techniques are preferred for stack characterization. Current interruption (CI) method is one of the most widely used techniques for ohmic resistance evaluation within electrochemical systems because of the simple equipment required—provided its sufficiently response time—and easiness of data analysis. The principle is to measure the transient cell voltage response to a CI. Ohmic resistance (R_Ω in $\Omega{\cdot}cm^2$) is determined by the ratio of the voltage change (ΔV in V) and applied current density (i in A cm^{-2}): $R_\Omega = \Delta V/i$ [5]. CI has been used at the stack level to measure the ohmic resistance of the cells and to detect the less performing ones [6]. Then galvanostatic electrochemical impedance spectroscopy (GEIS) proved to be a reliable technique in stack investigation since it allows each individual cell of the stack to be characterized. Stack investigations focusing on impedance non-uniformity [7, 8], water management [9], or performance optimization [10] have been carried out using this method. Finally, chronopotentiometry (CP) with pulsed current was suggested as an alternative method to CV for ECSA evaluation in half-cells [11], single cell, and stack configuration [12]. Though validated by Lee et al., this recent technique requires more investigation on the experimental uncertainty by comparison with results given by better known techniques i.e., CV and LSV.

The aim of the paper is to establish an analogy between CV and CP, and then to apply these different techniques in single cell configuration for determination of hydrogen crossover and electrochemical active surface area. Then CP will be applied to a three-cell stack formed with formerly characterized single cells for simultaneous characterization of the cells and comparison, with a critical eye on the accuracy and the limits of the various techniques.

2 Materials and fuel cell operation

The membrane electrode assemblies used during these tests were commercial seven layers of MEAs composed of 18-μm-thick perfluorosulfonic acid (PFSA) ionomer membranes reinforced with expanded polytetrafluoroethylene (ePTFE), Pt/C electrodes with a catalyst loading of 0.4 mg cm^{-2}, and 310-μm-thick dual-layer carbon GDLs (SGL 30BC) including a macroporous carbon fiber paper and a carbon black microporous layer (MPL) were used. The geometric surface area of the MEA was 100 cm^2. The hydrophobic (PTFE)/carbon particles phase added acted as a binder. Both anode and cathode flowfields were triple serpentine designed and machined into composite graphite. The assemblies and the 100 cm^2 cell plates (UBzM, Ulm, Germany) were manually pressurized using a torque wrench at 5 N m.

Electrochemical characterization of the cells and the stack was carried out using various techniques described and discussed in the next section. In all cases, humidified nitrogen (99.99 % purity) and hydrogen (99.995 % purity) were supplied to the cathode and the anode, respectively, with a flow rate of 300 STP mL min^{-1} per cell. In single cell configuration, the gases were humidified passing through a heated bubbler tank filled with deionized water. For tests conducted in stacks, hydrogen was humidified by the same bubbler but nitrogen was humidified by mixing with water supplied by means of a peristaltic pump into an electrical submillimetric heat exchanger (Serv Instrumentation France). For both humidification systems, the relative humidity (RH) value of the humidified gases has previously been controlled to reach the expected level within 1 %. To prevent condensation, the reactant gas lines were heated five degrees above the cell temperature which has been maintained at 55 °C by circulation of hot deionized water within the assembly. During voltammetric or potentiometric measurements, the cathode acted as the working electrode (WE) while the anode served as the counter electrode (CE): since the overpotential of hydrogen oxidation occurring at the anode is negligible, the anode (CE) also served as the reference electrode, as done in previous papers [13].

For fuel cells operation for conventional operation or GEIS at fixed current density, air replaced nitrogen and was humidified at RH = 62 % using the same systems as for nitrogen, depending on whether single cell or stack configuration was worked. Hydrogen was, however, not humidified. Stoichiometric factors were fixed to 1.5 for hydrogen and 3 for air oxygen. As in the previous investigations [14, 15], the current density was fixed at 0.3 A cm^{-2} for tests in single cell or stack configuration.

Fuel cell temperature was maintained at 55 °C for all operations and pressure was kept to the ambient level. Electrical measurements were performed with a 3-channels potentiostat (VSP, Biologic®) associated with an 80 A booster (VMP3, Biologic®). All MEAs were conditioned in single cell configuration for 72 h at 300 mA cm^{-2} and then electrochemically characterized prior to stack assembly.

The stack consisted of three cells: the so-called "front cell" was the cell located close to the inlet and outlet gas manifold, whereas the "back cell" designates the cell mounted in the other side of the stack; the "middle cell" was inserted between the front and the back cell.

3 Presentation of electrochemical techniques for FC characterization

Conventional techniques for evaluation of hydrogen crossover and electrochemical surface area (ECSA) are LSV and CV, respectively. Nevertheless, these techniques are not appropriate in stacks as explained before; therefore, CP with successive positive and negative current pulses can be applied for ECSA evaluation in stack as suggested formerly [11, 12]. This section aims at presenting and discussing the principle of the various methods and their significance. The experimental protocol developed and employed in this work is also given.

3.1 Linear sweep and CV

Hydrogen crossover through the ionomeric membrane is usually evaluated by LSV at 2 mV s^{-1} in the 0.05–0.8 V voltage range, as reported by Inaba et al. [3]. This technique is suitable for single cell configuration. The chosen value for hydrogen crossover current density is the steady value obtained around 0.4 V, i.e., at the anode potential corresponding to mass transfer controlled oxidation. In our case, the experimental uncertainty on the measurement is evaluated to 0.1 mA cm^{-2} i.e., 10 % for a typical crossover value of 1 mA cm^{-2}.

CV is usually applied for ECSA estimation in single cells. Figure 1a exhibits CV profiles recorded at different sweep rates on a single 100 cm^2 PEM cell between 0.05 and 0.8 V. The profile of the curves emphasizes the various electrochemical processes occurring during potential scan: (i) double-layer charging (ii) oxidation of hydrogen crossover, and (iii) proton adsorption/desorption, the two first processes occuring in the entire voltage range. Hydrogen desorption occurs in a broad range of potential because different catalyst sites with different desorption energies are involved in the process due to the polycrystalline structure of Pt particles in PEMFC electrodes [16]. For estimation of ESCA, integration of the current peak is carried out from the onset potential V_{start} to $V_{plateau}$ corresponding to the flat minimum of the current density profile (Fig. 1b). $V_{plateau}$ is usually around 0.45 V. The potential range V_{start} to $V_{plateau}$ is often referred as domain for Hydrogen Underpotential Deposition, H_{upd} [17]. Integration of the current in this potential range and after subtracting the contribution for double-layer charging measured at $V_{plateau}$ yields the charge for hydrogen desorption ($Q_{H/Pt}$ in C). The electrochemical surface area of the working electrode, ECSA (in cm^2 Pt cm^{-2}), is deduced from the above charge, using the following equation:

$$\mathrm{ECSA} = \frac{Q_{H/Pt}}{SQ_{H,A}} \tag{4}$$

where the specific charge $Q_{H,A}$ is equal to 210 μC cm^{-2}, value usually considered for oxidation of a monolayer of the adsorbed hydrogen on polycrystalline Pt and S is the electrode surface area. The value of the desorption charge obtained from CV measurement depends on the sweep rate [4]. The often recommended value of 30 mV s^{-1} has been used in this work.

The experimental uncertainty on ECSA measured by CV is mainly accounted for (i) adsorption of other species (notably carbon support products) than hydrogen and (ii) partial charge transfer between the adsorbed species and the catalyst [16]. Previous studies dealing with ECSA measurements in PEMFC [18, 19] estimated the experimental uncertainty on hydrogen desorption charge measured by CV to 10 %. In our case the uncertainty could be estimated to 0.1 C i.e., below 5 % for a typical desorption charge value of 4.5 C.

When the anodic plateau is attained (Fig. 1a), the current densities related to oxidation of carbon support and catalyst are often considered negligible [20]. The measured current is then the sum of two contributions: double-layer charging and oxidation of hydrogen crossing the membrane. Double-layer charging is a capacitive process; therefore, the corresponding current density, i_{dc}, is the product of the double-layer capacitance (C_{dl} in F cm^{-2}) by the sweep rate (in V·s^{-1}):

$$i_{dc} = C_{dl} \cdot v \tag{5}$$

Thus, if i_{H2} is the hydrogen crossover current density and v the sweep rate; the total current measured at $V_{plateau}$, determined at the beginning of the anodic plateau, is the sum of the capacitive and the faradaic current:

$$i_{tot}(V_{plateau}) = i_{dc} + i_{H_2} = C_{dl}v + i_{H_2} \tag{6}$$

Thus, CV performed at different sweep rates yields the discrete variation of the current density measured at $V_{plateau}$, i_{tot}, with rate v. As shown by relation. (6), fitting the data to a linear regression leads to the double-layer capacitance (slope) and the hydrogen crossover current density (Y-intercept) of the characterized cell. In the Results section, comparison of hydrogen crossover obtained by LSV and CV will be discussed.

However, a zoomed view of the voltammograms of Fig. 1a in the range 0.25–0.7 V reveals a slight, however, noticeable variation of the current above 0.45 V (Fig. 1b), which indicates the occurrence of other reactions: direct

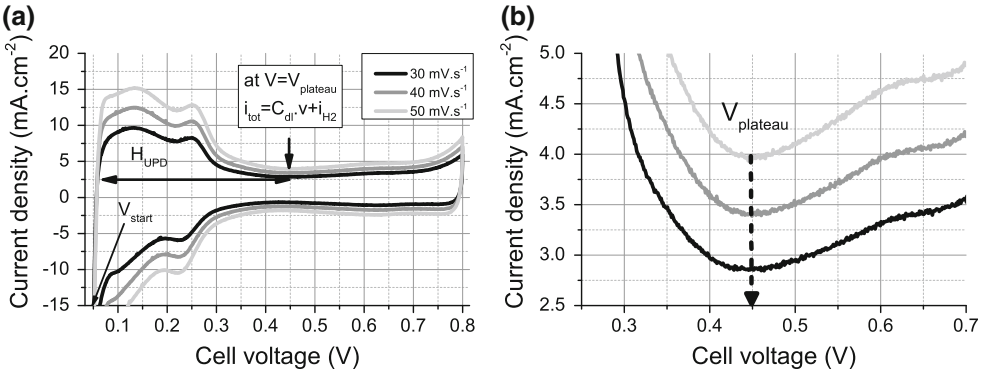

Fig. 1 **a** Cyclic voltammetry performed on a 100 cm^2 MEA fed with N_2/H_2 (300 STP mL min^{-1}) at 30, 40, 50 mV s^{-1} and **b** zoomed view of the voltammogramms between 0.25 and 0.7 V

oxidation of platinum or corrosion of the carbon support is probably of negligible significance below 0.55 V [20] but occurrence of electrochemical reversible reactions involving surface groups of the carbon support may be considered. Only relation (6) would then be approximate, leading to errors in determination of C_{dl} and i_{H2}, in particular for potentials larger than $V_{plateau}$. Therefore, it was preferred to evaluate these two parameters at fixed potential, $V_{plateau}$.

As a preliminary test, CV was performed with a three-cell stack at 200 mV s^{-1} (Fig. 2). As previously mentioned, the application of a potential ramp across the stack leads to an uneven distribution of the potential variations between the stack cells. The back cell, being far from the inlet and outlet manifolds, was found to exhibit more significant and faster potential variation than the two others. In particular, between 0.05 and 0.45 V, i.e., in the H_{upd} domain the sweep rate was estimated to be 47, 51, and 88 mV s^{-1} for the front, middle, and back cell, respectively. Thus, since hydrogen desorption charge is dependent on the sweep rate [4], CV performed on a stack cannot lead to comparable ECSA evaluation of the cells as the sweep rate in the H_{udp} domain differs from one cell to another.

3.2 Chronopotentiometry

3.2.1 Potentiometric method

As suggested by the previous studies [11, 12], the single cells were submitted to alternative current pulse of the same absolute intensity: the positive step causes the rise of the cell voltage. The current is manually reversed as soon as the cell voltage attained a limit fixed at 0.8 V to avoid damage of the electrode: the voltage then decreases until reaching a steady level below 0.1 V. The following cycle is rapidly started to avoid side accumulation of molecular hydrogen which could alter measurements in the following cycle.

Once characterized, the three single cells were assembled in a stack on which CP was performed with current densities ranging from 4 to 10 mA cm^{-2}. The stack voltage

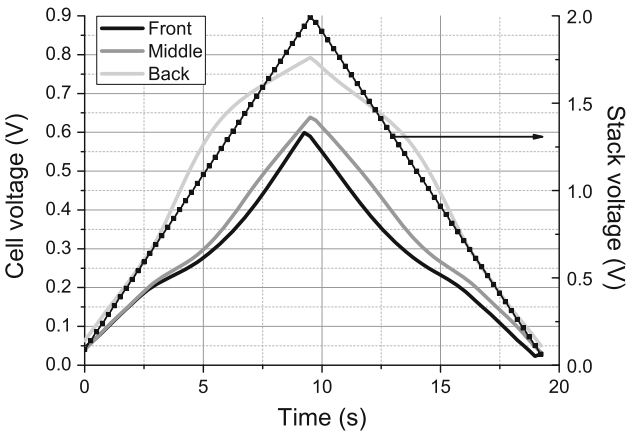

Fig. 2 Potential ramp (200 mV s^{-1}) applied on a three-cell stack (100 cm^2 MEA) fed with N_2/H_2 (300 STP mL min^{-1} *per cell*) corresponding cell voltage responses

was limited to 2.2 V to preserve the cells from high voltages.

The chosen sweep rate for CV tests to evaluate ECSA was fixed at 30 mV s^{-1}, following the previous investigations with fuel cell characterization and aging [14, 15]. In order to compare CV and CP techniques, it was, therefore, necessary, for CP, to find the right current density for which the voltage sweep rate in the H_{upd} zone is close to 30 mV s^{-1}. Preliminary tests led us to consider current density ranging from 4 to 10 mA cm^{-2} (Fig. 3): CP tests carried out in single cell led to sweep rate in the first domain, ΔV_1, ranging from approx. 15 to 40 mV s^{-1} in all cases; the chosen value to attain 30 mV s^{-1} was usually obtained for current density pulses in the order of 8 mA cm^{-2}.

3.2.2 Theory

Stevens et al. [11] demonstrated the possibility to convert potential versus time data obtained from galvanostatic measurements into differential capacity values, i.e., the relative change of the charge Q (C) with respect to potential V by using the approximation shown below:

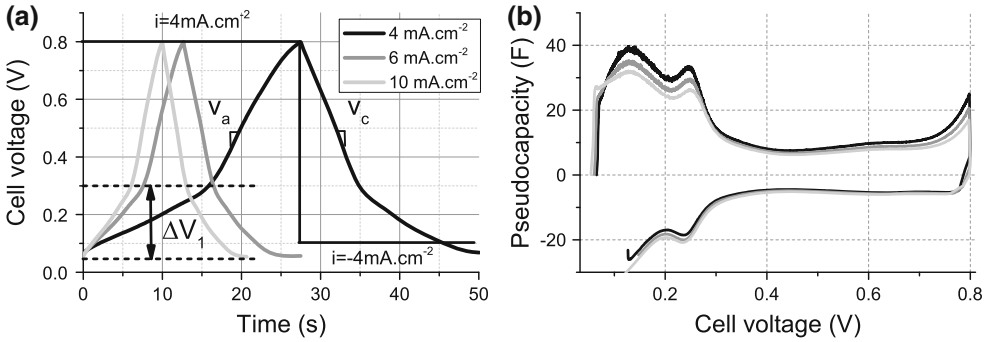

Fig. 3 Voltage versus *time curve* **a** and corresponding capacitive plot **b** of a PEMFC electrode during CP for the three single cells studied at different current density levels

$$\frac{dQ}{dV} \approx \frac{\Delta Q}{\Delta V} = \frac{iS\Delta t}{\Delta V} \tag{7}$$

where i is the applied current density (A cm^{-2}) and S is the electrode surface (cm^2). Differential capacity data or pseudocapacitance [4, 11, 17] (in C V^{-1} or F) are equivalent for CV measurements to the current normalized by the sweep rate (in A/(V·s^{-1}) or F). During galvanostatic measurement (CP, CP), in the H_{UPD} zone the differential charge dQ_{tot} recorded during elementary time period dt with applied current density i_a is composed of three terms [12] :

$$\begin{aligned} dQ_{tot} &= i_a dt = dQ_{H/Pt} + dQ_{dl} + dQ_{H_2} \\ &= C_{H/Pt}(V)dV + C_{dl}dV + i_{H_2}Sdt \end{aligned} \tag{8}$$

The left-hand term corresponds to the differential charge due to hydrogen electrosorption, $C_{H/Pt}$ being the corresponding voltage-dependent capacitance. The second term is for the double-layer charge of the electrode surface whereas the last term on the right hand expresses the faradaic charge for the oxidation of crossovered hydrogen. The above relation can be expressed as:

$$\frac{dQ_{tot}}{dV} = C_{H/Pt}(V) + C_{dl} + i_{H_2}S\frac{dt}{dV} \tag{9}$$

Figure 3a exemplifies the time variation of the cell voltage during CP carried out with alternative current pulses for various amplitudes of the current steps, after the experimental protocol Sect. 3.2.1. The corresponding DC plots calculated by using relation (7) are shown in (Fig. 3b). The time period required for the scan decreases with increasing current density (Fig. 3a). The period during which the current is positive is longer than the second phase of the cycle because the effective current ($i_{eff} = i_A + i_{H_2}$) is lower. Indeed, for an applied current density of ± 7 mA cm^{-2} and a crossover current of -1 mA cm^{-2} (the electrons from hydrogen oxidation leaves the working electrode), the effective current is 6 and -8 mA cm^{-2} during the anodic and cathodic phase, respectively.

Moreover, the increase in cell voltage resulting from the positive current steps exhibits three linear regions as follows. The first section for potentials below V_1—in the order of 0.3 V—corresponds to part of the H_{upd} domain; over this potential, a sharper increase is observed, before the rate of increase becomes again lower over 0.6 V or so. The corresponding slopes in the three parts of the increasing profile are equivalent to sweep rates; rate v_1 was defined as the sweep rate of the first section ($V < V_1$).

Figure 3b shows the capacitive plots deduced from CP for one of the cells investigated at various current density levels. It can be observed that similar profiles highlighting the previously mentioned electrochemical processes have been obtained with CV (Fig. 1a). The DC curves corresponding to lower current densities seem to be shifted toward positive values. This might be explained with equation (9): while the first and second terms exhibit no dependence on the sweep rate, the third term corresponding to hydrogen crossover oxidation capacitance varies with the reciprocal of the sweep rate which is lower at small current densities.

According to our hypothesis, at $V = V_{plateau}$ hydrogen desorption is over and only double-layer charging and oxidation of crossovered hydrogen occurs. Thus, if C_a is the pseudocapacitance (in F) during the anodic sweep and v_a is the instantaneous voltage sweep rate (see Fig. 3a), the following relation holds:

$$C_a = \frac{S \cdot i_{H_2}}{v_a} + C_{dl} \tag{10}$$

Likewise, for the cathodic plateau, just before the onset of hydrogen adsorption:

$$C_c = \frac{S \cdot i_{H_2}}{v_c} + C_{dl} \tag{11}$$

Similar to what have been shown in Sect. 3.1, linear regression of the C_a versus $1/v_a$ plot leads to determination of double-layer capacitance C_{dl} (Y-intercept) and hydrogen crossover current density i_{H2} (slope). Anodic pseudocapacitance was chosen to be plotted because the desorption charge is less affected by

adsorbing species and lead to the best approximation of the ECSA [4, 12]. Once these parameters are evaluated, integration of (8) in the H_{UPD} zone (V_{start}—$V_{plateau}$) allows the respective charges related to the different electrochemical processes to be determined. In particular, hydrogen desorption charge ($Q_{H/Pt}$) and thus ECSA can be estimated (relation (4)). If Δt is the time for the cell voltage to reach $V_{plateau}$ from V_{start}, and Q_{tot} is the total charge recorded during this time, integration of (8) between V_{start} and $V_{plateau}$ gives:

$$Q_{H/Pt} = Q_{tot} - C_{dl}(V_{start} - V_{plateau}) - i_{H_2}.S.\Delta t \quad (12)$$

The experimental error made on the evaluation of this charge may be expressed differentiating the previous expression:

$$\Delta Q_{H/Pt} = \Delta Q_{tot} + \left(V_{plateau} - V_{start}\right).\Delta C_{dl} + S[\Delta i_{H_2}\Delta t + i_{H_2}\Delta(\Delta t)] \quad (13)$$

The experimental error made on Q_{tot} and Δt are very small and lower than 10^{-2} C and 10^{-2} s, respectively, because these parameters are measured by the potentiostat. The estimation of the uncertainty on i_{H2} and C_{dl} is detailed in the next section.

3.2.3 Uncertainty on i_{H2} and C_{dl}

Double-layer capacitance and hydrogen crossover are parameters estimated from the slope and the *Y*-intercept, respectively, of linear regression. Error made on their estimation depends on the standard deviation on abscissa and ordinate data (σ_x and σ_y), regression coefficient (R^2), and the number of points of the fitted plot (n). Errors on the slope and *Y*-intercept (ε_{slope} and $\varepsilon_{Y\text{-intercept}}$) are then defined as follows [21]:

$$\varepsilon_{slope} = \frac{\sigma_y\sqrt{(1-R^2)}}{\sigma_x\sqrt{n-2}} \quad (14)$$

$$\varepsilon_{Y-intercept} = \frac{\sigma_y\sqrt{(1-R^2)\sum x_i}}{\sigma_x\sqrt{n-2}} \quad (15)$$

where x_i is the ith value of $1/v_a$ in the plot. These errors can be estimated for each linear regression performed on CV or CP data to evaluate the uncertainty on the measurements.

4 Results

In this part, conventional techniques, LSV and CV, were applied to three freshly conditioned single cells. Hydrogen crossover obtained by these two techniques are compared and discussed. Results obtained by CP in single cell are also presented and compared for the first time to the results obtained previously by CV and LSV; then, they are to be compared to those obtained once the single cells are assembled in stack.

4.1 LSV and CV in single cell configuration

Figure 4a shows the current measured at $V_{plateau}$ during CV performed on three single cells at three different sweep rates (30, 40, and 50 mV s^{-1}). As explained in sect. 3.1 with relation (6), a linear dependence is observed. Linear regression allowed evaluation of the variation slope and the *Y*-intercept corresponding to double-layer capacitance and hydrogen crossover current density, respectively. Linear fitting is shown for the front cell solely for clarity reason. Relative error on the evaluation of these parameters were calculated from (14) and (15) and were found to be 3 and 5 %, respectively. Comparison with the values obtained from LSV measurements shows that crossover results are in good agreement. CV results for C_{dl} (slope of the linear regression) and ECSA evaluation are compared with CP data in the next section.

4.2 CP in single cell configuration

CP performed at different current density levels allowed evaluation of anodic pseudocapacitance (C_a) and instantaneous sweep rate at $V_{plateau}$ (v_a). C_a versus $1/v_a$ plot (Fig. 5) exhibited good linear behavior ($R^2 > 0.99$). Linear fitting led to double-layer capacitance (C_{dl}) and hydrogen crossover current density (i_{H2}) determination. Data for one cell only were plotted for clarity reason. Values were found to be 5.54 F and 1.17 mA cm^{-2} with a relative error inferior to 2 %. These results are consistent with the LSV and CV data taking into account the uncertainty on the different estimations.

Table 1 shows the parameter values evaluated by the different techniques and the corresponding errors estimated on their measurement. Double-layer capacitance and crossover values show good agreement within around 5 % and 10 %, respectively, between the different techniques.

Once C_{dl} and i_{H2} evaluated, the respective charge in the H_{UPD} zone can be evaluated with (12) and plotted as a function of current density (Fig. 6). As explained before, since sweep rate increases with increasing current densities, the total measured charge decreases because of the shorter time period for oxidation of crossovered hydrogen. On the other hand, the charge for double-layer formation varies little with the applied current density. Hydrogen desorption charges are discussed below.

Hydrogen desorption charge was plotted as a function of the applied current density with error bars calculated from (14) to (15) (Fig. 7). $Q_{H/Pt}$ increases with the applied current pulses and, therefore, with the sweep rate which is in agreement with the results by Chaparro et al. [4] who attributed the observed dependency on adsorbing species related to carbon support reactivity. Uncertainty on $Q_{H/Pt}$ was evaluated from (13) to 0.05 C whatever the current

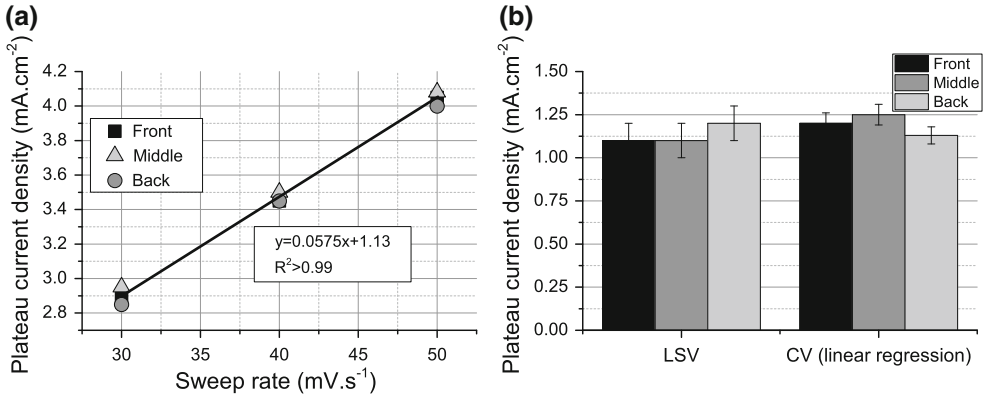

Fig. 4 **a** Plateau current density obtained from CV measurements at different sweep rates and **b** crossover current density estimated from LSV and CV

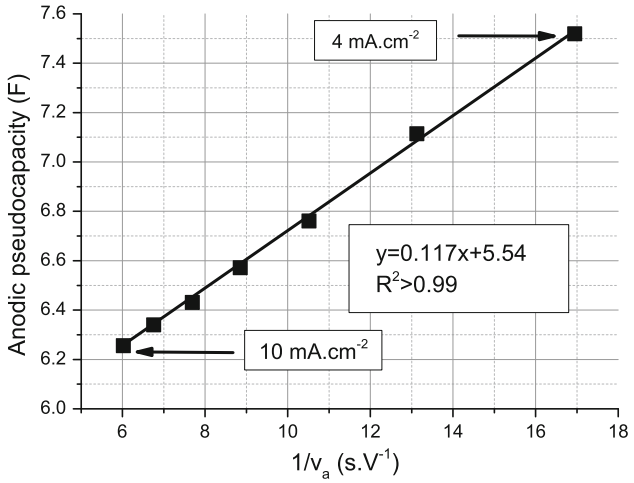

Fig. 5 Anodic pseudocapacitance as a function of the reciprocal of the instantaneous sweep rate at $V_{plateau}$ for CP performed from 4 to 10 mA cm^{-2} on a 100 cm^2 single cell (*front cell*)

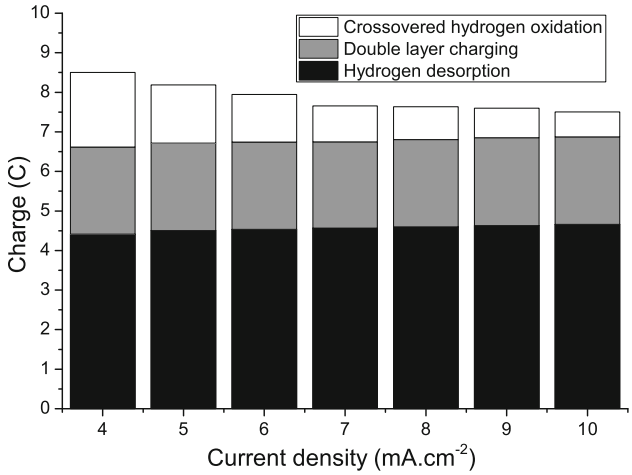

Fig. 6 Effect of the applied current density in CP runs on the respective charges related to the various electrochemical processes occurring during hydrogen desorption on Pt electrodes

Table 1 Double-layer capacitance and hydrogen crossover current determined from CV (30 mV s^{-1}), CP (8 mA cm^{-2}), and LSV (2 mV s^{-1})

	C_{dl} (in *F*)		*i* H_2 (in mA cm^{-2})		
	CV (3 %)	CP (<2 %)	CV (5 %)	LSV (10 %)	CP (<2 %)
Front	5.75	5.54	1.13	1.2	1.17
Middle	5.65	5.60	1.25	1.1	1.21
Back	5.75	5.63	1.13	1.1	1.19

Relative error estimated for the different techniques are indicated in brackets

density. At 8 mA cm^{-2}, hydrogen desorption charge was found to be 4.6 ± 0.05 C which is in agreement with the value obtained by CV (4.5 ± 0.1 C). The corresponding ECSA value, evaluated with (4), is 215 (±5) cm^2 Pt cm^{-2}.

4.3 CP in stack configuration

Once conditioned and characterized in single cell configuration, the MEAs were assembled in a stack that was operated for few hours at 0.3 A cm^{-2} for steady hydration of the membranes. Then ECSA and hydrogen crossover of the cells were evaluated by CP. The results obtained in stack configuration were compared to those obtained by CP measurements in single cell (Sect. 4.2). As explained before, for legitimate comparison, sweep rate values during H_{UDP} must be close to 30 mV s^{-1}. The cell responses to pulsed current density were shown to be very similar to each other. An example is given in Fig. 8, the sweep rate, in the domain ΔV_1, is approx. 30 mV s^{-1} for an applied current density of 9 mA cm^{-2}.

Similar to what have been done in single cell configuration, the crossover and the double-layer capacitance of the individual cells were first determined by linear

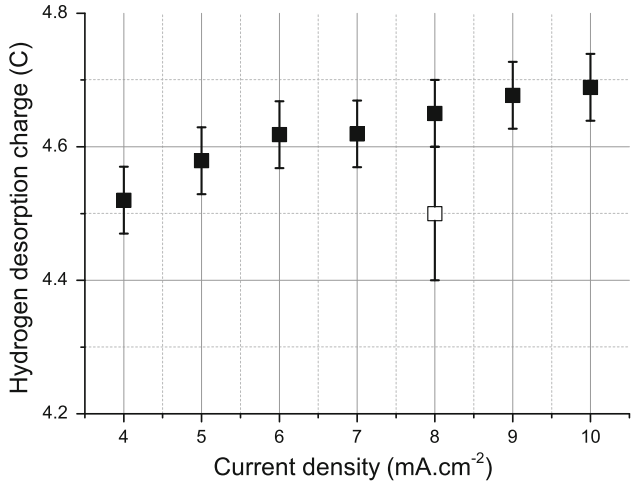

Fig. 7 Hydrogen desorption charge as a function of the current density. Charge given by CV is indicated by a white symbol

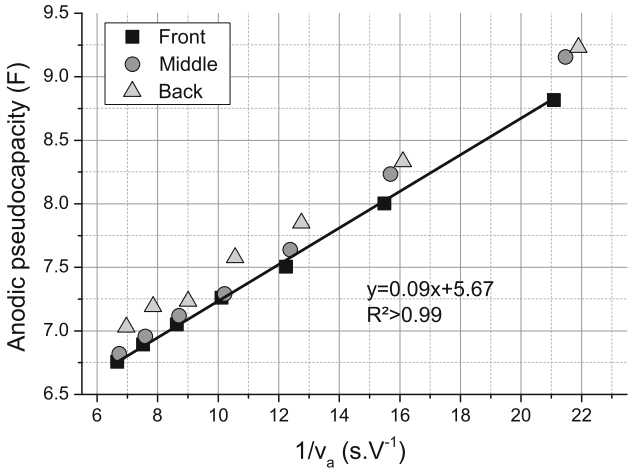

Fig. 9 C_a as a function of the reciprocal of the instantaneous sweep rate at $V_{plateau}$ for CP performed from 4 to 10 mA cm^{-2} on the stack

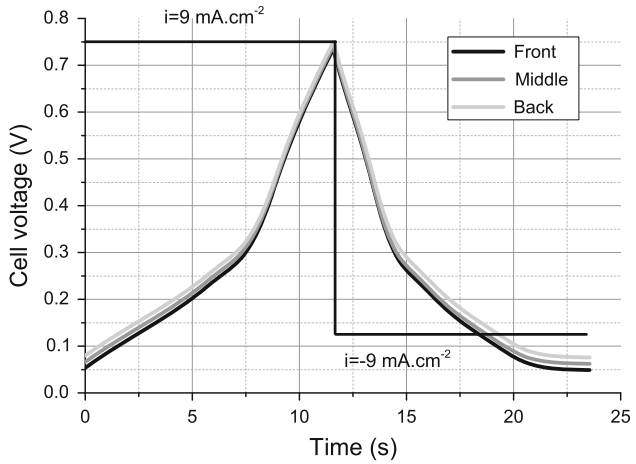

Fig. 8 Transient variation of the cell voltage of the three 100 cm^2 cells forming the stack in CP runs at 9 mA cm^{-2}

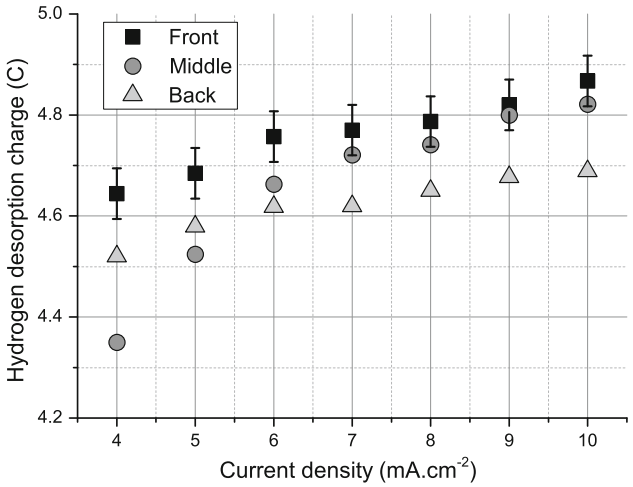

Fig. 10 Hydrogen desorption charge estimated for the stack cells as a function of applied current density

regression of C_a versus $1/v_a$ plot (Fig. 9). Only one regression is plotted for the sake of clarity. Results are in good agreement with the values obtained in single cell configuration (data shown for the Front cell in Fig. 5). Relative uncertainty on the parameters determined by linear regression was evaluated to be below 2 %.

As observed in single cell configuration, the values of $Q_{H/Pt}$ determined in the stack are also slightly increasing function of the intensity of the current peak (Fig. 10), with deviation between the cells below 5 %. The error bars were plotted for one cell solely for clarity reasons. Uncertainty on hydrogen desorption charge was equal to the value estimated in single cell configuration, around 0.05 C.

Finally, the ECSA values were determined in the stack with relation (4) and compared to those obtained by CV and CP in single cell configuration. In general manner, ECSA (Fig. 11a) shows a good agreement between the three sources of data, taking into account the uncertainty in the various techniques. Replicate tests and analysis of the interpretation technique indicates that the overall uncertainty in ECSA determination is below 5 %. Crossover values determined from CP in single cell and stack configuration show good agreement (Fig. 11b). ECSA values determined by CP in stack are in agreement with the results obtained from CP and CV in single cell configuration which validates CP as a technique for ECSA determination within a stack.

5 Conclusion

Different electrochemical techniques were performed in single cell and stack assembly to evaluate double-layer capacitance, hydrogen crossover, and electroactive surface

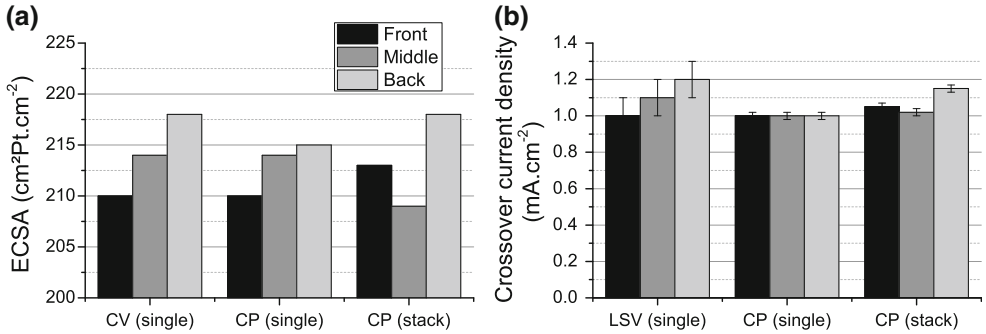

Fig. 11 **a** Comparison of ECSA and **b** hydrogen crossover of the 100 cm^2 MEAs, depending on the electrochemical technique employed

area. The uncertainty on the determination of these parameters from the different techniques was either estimated (LSV) or calculated (CV and CP). Error on the determination of these parameters from linear regression is very small (inferior to 5 %) leading to small uncertainty in ECSA evaluation. Comparison of the different parameters with respect to the error made on their evaluation shows that the various values are in agreement. CV and CP performed for ECSA evaluation in different configurations (single cell and stack) show consistent results taking into account the uncertainty on the measurements.

CP was validated here as a method for ECSA determination for PEM fuel cells. Contrary to CV, this technique can be used in stack configuration which provides a powerful tool to monitor ECSA loss of the stack cells during the long-term operation. However, as the quality of the measurement may depend on the cell number in the stack, characterization limits of systems with higher cell number and/or containing defective cell(s) should be investigated as the voltage response discrepancy between the different cells may be larger.

References

1. Bonnet C, Franck-Lacaze L, Huang B et al (2012) Aging of polymer electrolyte membrane fuel cells (PEMFC): general features and investigation of two typical examples. J Appl Electrochem 42:699-–709. doi:10.1007/s108000120451z
2. De Bruijn FA, Dam VAT, Janssen GJM (2008) Review: durability and Degradation Issues of PEM fuel cell components. Fuel Cells 8:3–22. doi:10.1002/fuce.200700053
3. Inaba M, Kinumoto T, Kiriake M et al (2006) Gas crossover and membrane degradation in polymer electrolyte fuel cells. Electrochim Acta 51:5746–5753. doi:10.1016/j.electacta.2006.03.008
4. Chaparro AM, Martín AJ, Folgado MA et al (2009) Comparative analysis of the electroactive area of Pt/C PEMFC electrodes in liquid and solid polymer contact by underpotential hydrogen adsorption/desorption. Int J Hydrog Energy 34:4838–4846. doi:10.1016/j.ijhydene.2009.03.053
5. Cooper KR, Smith M (2006) Electrical test methods for on-line fuel cell ohmic resistance measurement. J Power Sour 160:1088–1095. doi:10.1016/j.jpowsour.2006.02.086
6. Mennola T, Mikkola M, Noponen M et al (2002) Measurement of ohmic voltage losses in individual cells of a PEMFC stack. J Power Sour 112:261–272. doi:10.1016/S0378-7753(02)00391-9
7. Diard J-P, Glandut N, Le Gorrec B, Montella C (2004) Impedance Measurement of Each Cell of a 10 W PEMFC Stack under Load. J Electrochem Soc 151:2193. doi:10.1149/1.1815152
8. Yuan X, Sun JC, Blanco M et al (2006) AC impedance diagnosis of a 500 W PEM fuel cell stack: part I: stack impedance. J Power Sour 161:920–928. doi:10.1016/j.jpowsour.2006.05.003
9. Yousfi-Steiner N, Moçotéguy P, Candusso D, Hissel D (2009) A review on polymer electrolyte membrane.fuel cell catalyst degradation and starvation issues: causes, consequences and diagnostic for mitigation. J Power Sour 194:130–145. doi:10.1016/j.jpowsour.2009.03.060
10. Yan X, Hou M, Sun L et al (2007) AC impedance characteristics of a 2 kW PEM fuel cell stack under different operating conditions and load changes. Int J Hydrog Energy 32:4358–4364. doi:10.1016/j.ijhydene.2007.06.024
11. Stevens DA, Dahn JR (2003) Electrochemical characterization of the active surface in carbon-supported platinum electrocatalysts for PEM fuel cells. J Electrochem Soc 150:770–775. doi:10.1149/1.1573195
12. Lee K-S, Lee B-S, Yoo S-J et al (2012) Development of a galvanostatic analysis technique as an in situ diagnostic tool for PEMFC single cells and stacks. Int J Hydrog Energy 37:5891–5900. doi:10.1016/j.ijhydene.2011.12.152
13. Gasteiger HA, Kocha SS, Sompalli B, Wagner FT (2005) Activity benchmarks and requirements for Pt, Pt-alloy, and non-Pt oxygen reduction catalysts for PEMFCs. Appl Catal B Environ 56:9–35. doi:10.1016/j.apcatb.2004.06.021
14. Huang BT, Chatillon Y, Bonnet C et al (2012) Experimental investigation of air relative humidity (RH) cycling tests on MEA/cell aging in PEMFC part I: study of high RH cycling test with air RH at 62 %/100 %. Fuel Cells 12:335–346. doi:10.1002/fuce.201100060
15. Huang BT, Chatillon Y, Bonnet C et al (2012) Experimental investigation of air relative humidity (RH) cycling tests on MEA/cell aging in PEMFC part II: study of low RH cycling test with air RH at 62 %/0 %. Fuel Cells 12:347–355. doi:10.1002/fuce.201100061
16. Trasatti S, Petrii OA (1992) Real surface area measurements in electrochemistry. J Electroanal Chem 327:353–376. doi:10.1016/0022-0728(92)80162-W
17. Bard AJ, Faulkner LR (2001) Electrochemical methods: fundamentals and applications. Wiley, New York

18. Benitez R, Chaparro AM, Daza L (2005) Electrochemical characterisation of Pt/C suspensions for the reduction of oxygen. J Power Sour 151:2–10. doi:10.1016/j.jpowsour.2005.02.077
19. Pozio A, De Francesco M, Cemmi A et al (2002) Comparison of high surface Pt/C catalysts by cyclic voltammetry. J Power Sour 105:13–19
20. Roen LM, Paik CH, Jarvi TD (2004) Electrocatalytic corrosion of carbon support in PEMFC cathodes. Electrochem Solid-State Lett 7:19–22. doi:10.1149/1.1630412
21. Kenney JF (1964) Mathematics of statistics, 3rd edn. Van Nostrand, New York